*Bull. Spec. Astrophys. Obs.*, 1998, 44, 119–126

# Telescope resolution enhancement through the pupil segmentation

**Pluzhnik E.A.**[a,b], **Balega Yu.Yu.**[a], **Vasyuk V.A.**[a], **Maximov A.F.**[a]

[a] Special Astrophysical Observatory of the Russian AS, Nizhnij Arkhyz 357147, Russia
[b] Astronomical Observatory of the Kharkov University, Sumskaya str. 35, Kharkov, 310022, Ukraine

*Received October 8, 1997; accepted November 10, 1997.*

**Abstract.** Experimental results of the pupil segmentation at the SAO 1 m telescope are presented. It is shown that by using the segmentation system the angular resolution can be improved at the sites with average seeing conditions. Using 10% of the best selected short-exposure images and their subsequent recentering, images of the binary star $\gamma$ Vir were obtained with a resolution of 1.″9 under the 4.″3 seeing, and 0.″9 under the 1.″1 seeing. It is shown that the acquisition of correlation functions for the pupil segmentation system with an optimum selected sub-pupil size yields higher signal-to-noise ratio in an image.

**Key words:** Instrumentation: methods – high resolution imaging

## 1. Introduction

In the optical region of the spectrum the constraints on the angular resolution of astronomical observations are due to the blurring and motion of images caused by distortions of the wave front in the turbulent atmosphere and by the imperfect telescope tracking. The time scale of the phase fluctuations of the optical wave lies within 1–50 ms. If the image motion is compensated, the angular resolution of the telescope first grows with increasing its diameter $D$, reaching a maximum at $D/r_0 = 3.7$, where $r_0$ is the Fried parameter determining the state of the atmosphere (Fried, 1966). As $D$ is further increasing, the resolution decreases. The image of a point source produced by a large-diameter telescope is blurred into a spot $\lambda/r_0$ in size.

The resolution can be improved through selection of the best short exposure images consequently summing them up. The probability of obtaining the diffraction-limited image quality at $D/r_0 \geq 3.5$ is determined by expression: Prob$\sim 5.6\exp[-0.1557(D/r_0)^2]$ (Fried, 1978). It also drops fast with increasing $D/r_0$. For instance, if 10% of the best images are selected and reduced to a common photocenter, at $D/r_0 = 5$ the theoretical gain in resolution will then be equal to 3.1, while at $D/r_0 = 10$ it will be as low as 2.4 (Hequet and Coupinot, 1985). For large instruments, $D/r_0$>10, the probability of finding an image with a resolution 2–3 times the average becomes negligibly low.

At the BTA site, $r_0$ is rarely over 10 cm (this corresponds to $\approx 1''$ resolution). That is why, for the optimum application of the selection and recentering algorithms it is worthwhile to split the entrance pupil of the telescope into individual segments, $d\approx$30–40 cm in size, for which a maximum resolution can be achieved. Experiments with the application of a pupil segmentation system were first done with the 3.6 m telescope CFHT (Hawaii), which demonstrated the possibility of improving the resolution by a factor of 2–3 as against the classical version of full-pupil observations, with a sufficiently high limiting magnitude ($\sim 17^m$) (Lelievre et al., 1988; Sebag et al., 1990).

However, a number of problems related to the possibilities of the telescope pupil segmentation remain to be solved. Firstly, the observations on the Hawaiian telescope were conducted on the night with an exceptionally good seeing, when $r_0$ =30–40 cm. Therefore, the authors could use a small number of segments to break the 3.6 m telescope pupil into; each segment was comparable with a 1.1 m telescope. At other observing sites a larger number of subapertures of small size will be required and the efficiency of the technique will be reduced. Secondly, in the experiment done with the CFHT an exposure of 0.4–1 s was used, followed by the image fine structure blurring as a result of averaging. It is important to check how efficient the pupil segmentation is at 0.02 s exposures, "freezing" speckle images. Besides, the efficiency of the technique was avaluated at the CFHT as a result of simple summation of images formed by individual segments. It is basically determined by the recentering errors. The correlation analysis increases considerably the sensitivity of the method. To resolve

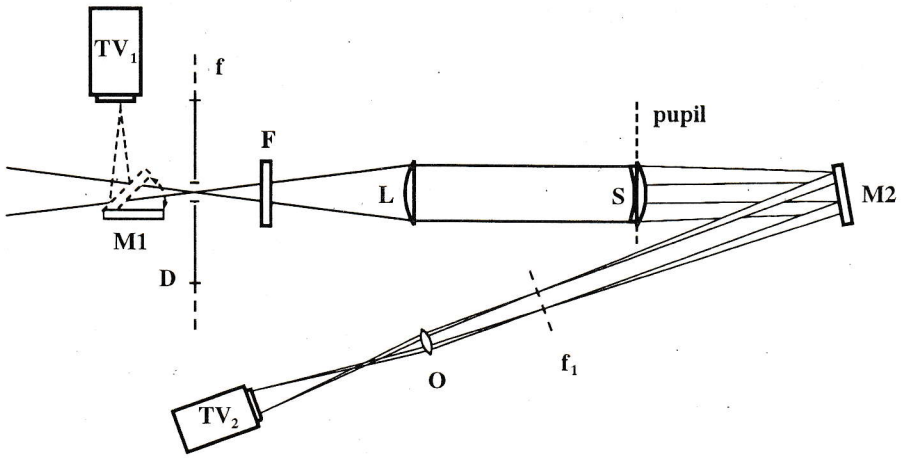


Figure 1: *The optical layout of the pupil segmentation system*

the problems mentioned, in 1996 we observed binary stars with the pupil segmentation system at the 1 m Zeiss-1000 telescope of SAO. Below we present a description of the optical layout of the experiment and technique, as well as the results of using the pupil segmentation for binary star imaging.

## 2. The pupil segmentation system

We have designed a segmentation system for the Cassegrain f:13.5 focus of the 1 m Zeiss-1000 telescope of SAO. The optical layout of the system is shown in Fig. 1. The pupil slicer S, whose parameters have been chosen to optimize the aperture diameter in resolution (the average value of $r_0$ is 5 cm), breaks up the telescope aperture into 18 segments of $d = 18$ cm. It incorporates a plane-convex lens with a focal length of 410 mm placed in the pupil plane with a set of cemented prisms A, B, C, whose angles of refraction are $11'$, $18'$ and $21'$, respectively (Fig. 2 a). The prisms are shaped as regular hexagons with a side of 4.5 mm with their vertexes oriented towards the center (to reduce chromatic aberration), while their bases are of oposite orientation. The pupil of the telescope is imaged by the lens L with a focal length of 338 mm. Unfortunately, the segments in the central region are partially screened by the telescope secondary mirror cell. The optical elements of the slicer have been manufactured by E.I. Perepelitsin in the workshop of SAO.

The photon counting television camera $TV_2$ (Balega and Ryadchenko, 1984) has a format of 256 × 256 pixels and the field 10 mm in size. With the scale $0''.133$/pixel this corresponds to an angular field of $6''.8$. The reserve in resolution is needed for accurate determination of the photocentres of images formed by individual segments.

On the scheme are also shown:

1) the field diaphragm D placed in the telescope focal plane f to avoid overlapping of images formed by different segments;
2) the filter wheel F;
3) the television camera $TV_1$ and the mirror M1 for pointing to an object;
4) the mirror M2 that breaks the beam to diminish the total length of the device (the optical path length is 1284 mm);
5) the microobjective O with magnification of $3.7^{\times}$ for fitting the scale at slicer focus to pixel size of the detector $TV_2$.

## 3. Observations and data processing

We carried out 1 m telescope observations with the segmented pupil on March 28 and May 8, 1996. For the observation we have chosen the binary star $\gamma$ Vir ($\rho = 1''.3$, m=2.74) with the small magnitude difference. The images were obtained through the interference filter of $\Delta\lambda$=200 Å centered at $\lambda$=6590 Å. The television acquisition system ensured real-time digitization of 8 frames per second. The time of individual exposures was 20 ms. During the March and May observations 5500 and 2000 instantaneous images were accumulated, respectively.

The primary processing of the data included photometric and geometric correction of each frame. In the next stage the collection of statistical information was performed, which included the definition of positions of photocentres of short-exposure images for individual segments, their quality grading and averaging of the centered instantaneous images. As an image quality criterion, a parameter equal to the ratio of the low-frequency and high-frequency parts of spatial spectrum energy of image $I(\omega)$ was used:

$$C_0 = \frac{\int_1 d\omega(|I(\omega)|^2 - N)}{\int_2 d\omega(|I(\omega)|^2 - N)}. \quad (1)$$

Here in the integral 1 the integration was performed

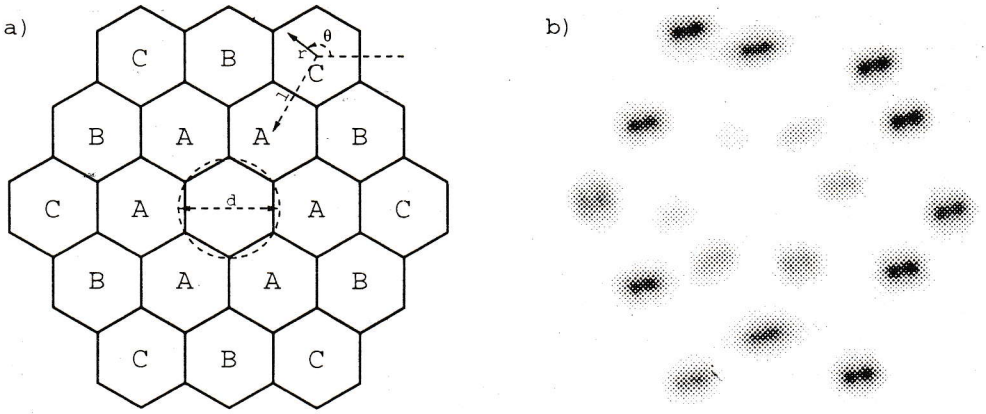


Figure 2: *a) The pupil slicer configuration;*
*b) the binary star image obtained with the pupil segmentation system; the deterioration of the images produced by the central segments is due to partial obscuration of the beam by the telescope secondary mirror cell.*

with respect to frequencies below the cut-off frequency of the atmosphere $\omega \leq 2\pi\lambda/r_0$, in the integral 2 – with respect to frequencies $\lambda/r_0 < \omega \leq 2\pi\lambda/d$, and the average value of $|I(\omega)|^2$ at frequencies above the segment cut-off frequency $2\pi\lambda/d$ gives the noise power spectrum estimation N. The offset $\boldsymbol{r}_c$ between the two images $i_1(\boldsymbol{r})$ and $i_2(\boldsymbol{r})$ is determined from the condition:

$$f(\boldsymbol{r}_c) = \frac{\int_1 d\omega(|I_1(\omega) + I_2(\omega)\exp(i\omega\boldsymbol{r}_c)|^2 - }{\int_2 d\omega(|I_1(\omega) + I_2(\omega)\exp(i\omega\boldsymbol{r}_c)|^2 - } \frac{-N_1 - N_2)}{-N_1 - N_2)}, \quad (2)$$

where the indices 1 and 2 refer to the first and second images, respectively. As compared to the usual recentering, such algorithm takes into account the fine structure of instantaneous images. To determine statistical properties of instantaneous and averaged images, instead of the parameter $r_0$, we used two parameters correlated with it: the diameter of a circle $d_{0.5}$ that contains half of energy in a point source image (for instantaneous images) and FWHM (for averaged images).

## 4. Determination of $r_0$

The best way to estimate the atmospheric seeing parameter $r_0$ is the computation of the wavefront angle-of-arrival structure function, which is determined as (Tatarski, 1967):

$$D_\alpha = \langle|\boldsymbol{\alpha}_1 - \boldsymbol{\alpha}_2|^2\rangle = 2\langle|\boldsymbol{\alpha}|^2\rangle - 2\langle(\boldsymbol{\alpha_1}, \boldsymbol{\alpha_2})\rangle, \quad (3)$$

where $\boldsymbol{\alpha}_1$ and $\boldsymbol{\alpha}_2$ are the fluctuations of the average wavefront tilt on segments 1 and 2, while $\sigma^2 = \langle|\boldsymbol{\alpha}|^2\rangle$ is the dispersion of image center motion. Such estimate is free from systematic errors of the telescope tracking and inaccurate guiding. For the segments of the same shape, the correlation function of the fluctuations of wavefront tilt is equal to (Tokovinin, 1988):

$$\langle(\boldsymbol{\alpha_1}, \boldsymbol{\alpha_2})\rangle = \frac{1}{2S}\left(\frac{\lambda}{2\pi}\right)^2 \int T(\mathbf{r})\Delta D_\varphi(\mathbf{r}+\mathbf{l})d\mathbf{r}, \quad (4)$$

where $T(\mathbf{r}) = S^{-1}\int P(\mathbf{r}')P(\mathbf{r}'+\mathbf{r})d\mathbf{r}'$ is the autocorrelation of the segment pupil function $P(\mathbf{r})$ divided by segment area $S$, $\mathbf{l}$ is the vector that connects the centers of segments, $\Delta = \frac{\partial^2}{\partial x^2} + \frac{\partial^2}{\partial y^2}$ is the Laplas operator, $D_\varphi(\mathbf{r}) = 6.88(r/r_0)^{\frac{5}{3}}$ is the phase structure function (Fried, 1966), and segment pupil function is equal to:

$$P(\mathbf{r}) = \begin{cases} 1 & \text{inside the segment} \\ 0 & \text{outside the segment.} \end{cases} \quad (5)$$

Under the assumption of Kolmogorov's turbulence model, expression (4) in the polar coordinate system $(r, \theta)$ (Fig. 2) takes the form:

$$\langle(\boldsymbol{\alpha_1}, \boldsymbol{\alpha_2})\rangle = 0.308 r_0^{-\frac{5}{3}}\left(\frac{\lambda}{d}\right)^2 \times \int T(r,\theta)[r^2 + l^2 + 2lr\cos\theta]^{-\frac{1}{6}} r dr d\theta. \quad (6)$$

For a circular segment (the result must be close for a hexagonal segment as well) in the case $l > d$, accurate expression for $\langle(\boldsymbol{\alpha_1}, \boldsymbol{\alpha_2})\rangle$ has the form:

$$\langle(\boldsymbol{\alpha_1}, \boldsymbol{\alpha_2})\rangle = 1.233\lambda^2 r_0^{-\frac{5}{3}} l^{-\frac{1}{3}} \sum_{k=0}^{\infty} a_k \left(\frac{d}{l}\right)^{2k}, \quad (7)$$

where $a_0 = \frac{\pi}{16}$, while

$$\frac{a_{k+1}}{a_k} = \frac{(k+\frac{1}{6})^2(2k+3)}{2(k+1)(k+2)(k+3)}.$$

The dispersion of image motion corresponding to this case is

$$\langle|\boldsymbol{\alpha}|^2\rangle = 0.339\lambda^2 d^{-\frac{1}{3}} r_0^{-\frac{5}{3}}. \quad (8)$$

Expressions (3), (7) and (8) make it possible to determine the Fried parameter $r_0$ from the measured angle-of-arrival structure function $D_\alpha$. Note that the result is strongly dependent on aberrations and defocusing of the optical system. The defocusing widens the point source image, which results in underestimation of the $r_0$ parameter when measured from the mean profile of the star. On the other hand, the defocusing reduces the image motion, giving the overestimated value for $r_0$ from the structure function measurement. Therefore, in order to derive correct $r_0$ value, the defocusing, at which the $r_0$ estimates for these methods of measurements coincide, should be introduced into the expressions for the mean profile and structure function. In Fig. 3 the experimental and theoretical structure functions of image motion for a segment are presented. They have been derived from the May observational results with allowance made for the defocusing. The Fried parameter measured in this way is equal to $3.12 \pm 0.02$ cm and $11.6 \pm 0.1$ cm for the March and May observations, respectively.

## 5. Statistical properties of individual images

In order that final resolution be limited only by diffraction on the segment, the selection rate of the number of instantaneous images must not exceed 0.026 for $d/r_0 = 5.76$ (March observations) and 0.999 for $d/r_0 = 1.55$ (May observations) (Fried, 1978). The theoretical and experimental density distribution of the resolution of short-exposure images obtained with the pupil segmentation system are markedly different (Fig. 4). The mean value of the parameter $d_{0.5}$ is 3.″23 for the March observations and 1.″37 for May. They

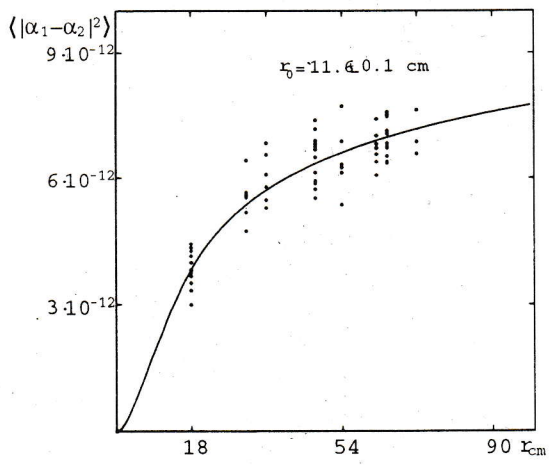


Figure 3: *The experimental (dots) and the theoretical (line) structure function of image motion for pupil d =18 cm at $r_0$ =11.6 cm with allowance made for defocusing of the optical system.*

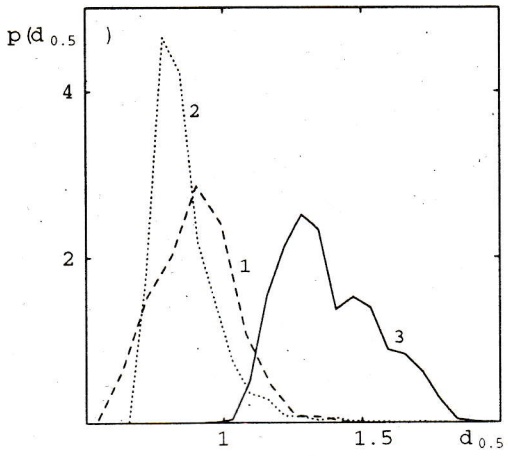


Figure 4: *Density distribution of the parameter $d_{0.5}$ from the series of short-exposure image for D=1m (1), 0.18m (2) (results of modelling) and D=0.18m (experiment) (3) at $r_0$=11.6cm.*

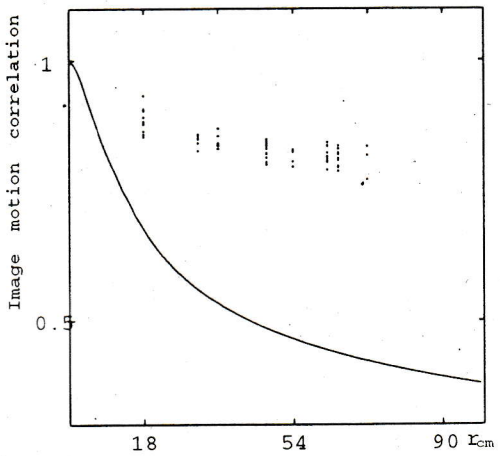


Figure 5: *The theoretical (line) and experimental (dots) relationship between the correlation coefficient of image motion (defocusing allowed for) and separation r between the segments*

are 1.11 and 1.59 times worse, respectively, than theoretical values (2.″91 and 0.″86) for a segment. With respect to the full aperture the mean value $d_{0.5}$ is by factor 1.08 smaller for the March observations (3.″5) and 1.54 times larger for the observations conducted in May (0.″89). The indicated discrepancy between the theoretical and experimental estimates may be due to the following:

- overestimated Fried radius $r_0$;
- considerable contribution of non-atmospheric factors, in particular, of optical aberrations, to image distortion.

As it is mentioned above, the method we use can lead only to underestimated values of $r_0$. The influence of the telescope tracking errors on the image

| | $FWHM_{dif}$ | $FWHM_{opt}$ | $\frac{\sigma_{tel}}{\sigma_{atm}}$ | $\frac{\text{Atm. SE}}{\text{Atm. LE}}$ | $\frac{FWHM_{SE}}{FWHM_{LE}}$ |
|---|---|---|---|---|---|
| Full pupil, $r_0$=11.6 cm | 0.″14 | – | – | $\frac{0.″65}{1.″14}$ | $\frac{0.″67}{1.″18}$ |
| Segmented pupil, $r_0$=11.6 cm | 0.″78 | 0.″94* | $\frac{<0.″07^*}{0.″52^*}$ | $\frac{0.″22}{1.″14}$ | $\frac{1.″00^*}{1.″48}$ |
| Full pupil, $r_0$=3.12 cm | 0.″14 | – | – | $\frac{3.″31}{4.″30}$ | $\frac{3.″31}{4.″33}$ |
| Segmented pupil, $r_0$=3.12 cm | 0.″78 | 0.″97* | $\frac{1.″81^*}{1.″29^*}$ | $\frac{1.″77}{4.″30}$ | $\frac{1.″88}{4.″77}$ |

Table 1: *The contribution of various factors to the image resolution for long (LE) and short (SE) exposures. Designated: the diffraction disk ($FWHM_{dif}$), the contribution of the optic ($FWHM_{opt}$), the mean-squared values of the atmospheric image wander ($\sigma_{atm}$) and telescope tracking errors ($\sigma_{tel}$), the contribution of the atmosphere (Atm. SE and Atm. LE), FWHM for short and long exposures. Experimental results are marked with an asterisk. All other values are theoretical estimates.*

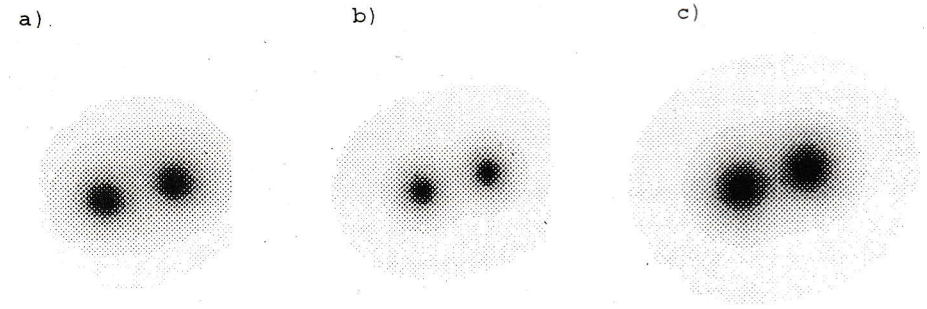


Figure 6: *) The image of $\gamma$ Vir produced by the segmentation system at $\tau = 10\%$ and $r_0$=11.6 cm;*
*b) the sum of short exposure images of $\gamma$ Vir for 1 m aperture (model);*
*c) long exposure image of $\gamma$ Vir for 1 m aperture (model).*

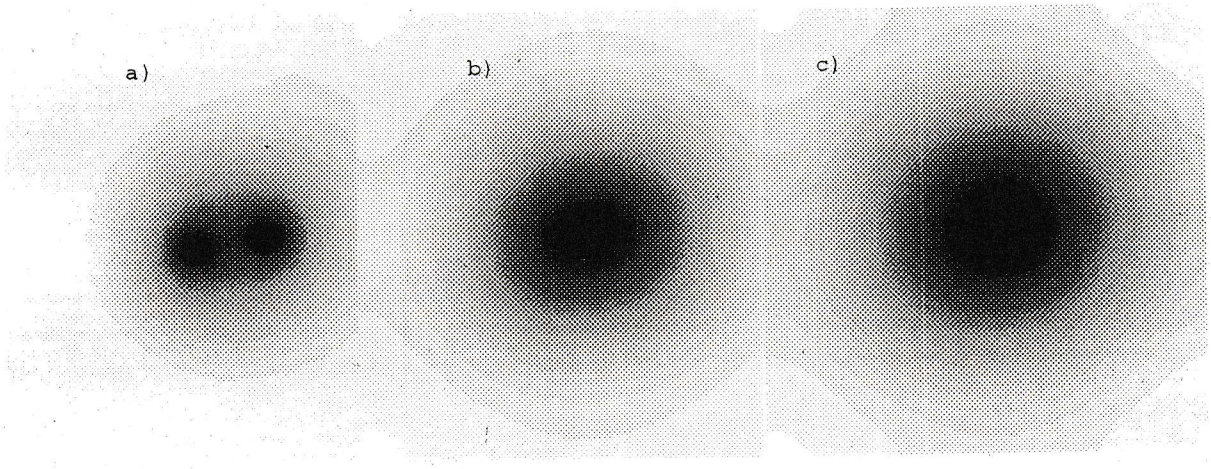


Figure 7: *The same as Fig. 6, but with $r_0$=3.12 cm and $\tau = 3\%$.*

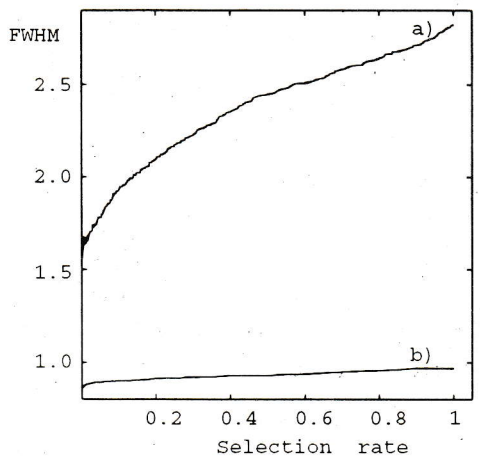


Figure 8: *The resolution versus the selection rate $\tau$ at $r_0$=3.12 cm () and $r_0$=11.6 cm (b).*

quality can be estimated from the departure of measured image motion from its theoretical values (Fig. 5, Table 1). The contribution of optical aberrations into resolution degradation (Table 1) is estimated from the difference in $r_0$ values received from image motion correlation and measured short-exposure transfer function.

The correlation coefficient $d_{0.5}$ between different segments is not higher than 0.16±0.02 (March observations). This means that the segmentation system may be considered as a set of telescopes operating independently, for which all the theoretical evaluations of efficiency available in the papers by Fried (1966) and Hequet and Coupinot (1985) are valid.

## 6. Imaging of the binary star $\gamma$ Vir

Images of the binary star $\gamma$ Vir obtained with the selection rate $\tau$=10% (May) and 3% (March), are presented in Fig.6 and Fig.7. Therein are also given the calculated images for the full aperture with the measured values of the Fried parameter. The seeing varied from FWHM = 4.″3 for the March observations ($r_0$ = 3.12 cm, poor seeing) to FWHM = 1.″14 for the May observations ($r_0$=11.6 cm, good seeing).

Because of aberrations, the images formed by individual segments are different. This is especially pronounced for inner pupil slicer segments, which are markedly vignetted by the secondary mirror cell. The distortion for the rest of the segments is likely to be caused by the inaccurate focusing. The resolution of different segments ranges from 1.″19 to 1.″68. Poor-quality segments were excluded from further analysis.

The resolution reached in the observations of binary $\gamma$ Vir for different $\tau$ is shown in Fig. 8. With a selection rate of 10% the resolution is 1.″92 and 0.″90 for the March and May observations, respectively, however, one should bear in mind here a considerable contribution of non-atmospheric factors to the deterioration of the image quality. Note also that for faint objects, with the high rate of selection, the resolution may prove to be strongly overestimated due to the small number of events recorded.

In Fig. 9 the experimental and theoretical relation between the gain in resolution and selection rate is shown. One should note that with a high selection rate the resolution gain values may be distorted by the error in the FWHM determination (especially for faint objects). The figure demonstrates a higher gain in the resolution for the real system as against the theoretical relationship at high enough selection rate. The reason for this is that in the absence of selection the real system yields a lower resolution than the theoretical resolution, whereas at high selection rate the resolution approaches the diffraction resolution. For the selection rate that ensures the diffraction resolution on a segment, the gain through selection is 1.65 and 1.13 with ratio $d/r_0$ equal to 5.76 (March) and 1.55 (May), respectively. The corresponding theoretical gains are 1.36 and 1.0.

The gain in the resolution of the segmentation system as compared to the theoretical resolution of the full aperture, under different selection rates, is given in Table 2. Note, that during the night of good seeing the relation between $r_0$, $D$ and $d$ decreased the gain in resolution of the segmentation system in comparison with the theoretical short-exposure resolution of the 1 m telescope.

All the estimates presented have been obtained with short exposures of 0.02 s. Since for technical reasons there was no possibility of concurrent resolution measurements for the full aperture, we made such estimates by numerical modelling under the assumption of Kolmogorov's turbulence model. In the modelling the Fried parameter values obtained from the observational data were used.

## 7. Correlation signal asquisition

The sensitivity of the pupil segmentation is restricted by recentering errors of short-exposure images. As it is known, the first- and the second-order correlation functions are independent of the shift of the image as a whole. Therefore the mean correlation functions do not depend on the object recentering errors. At the same time correlation functions enable an image restoration (Weigelt, 1991; Pluzhnik, 1996). At high selection rates one can get nearly diffraction limited images. In this case there is no need to consider the mean optical transfer function of the system for the estimation of the object's correlation function. As a result, the stability of reconstruction algorithms is increasing. It also follows that for the resolution of the segmentation system with the correlation signal acquisition the estimates given in the previous sec-

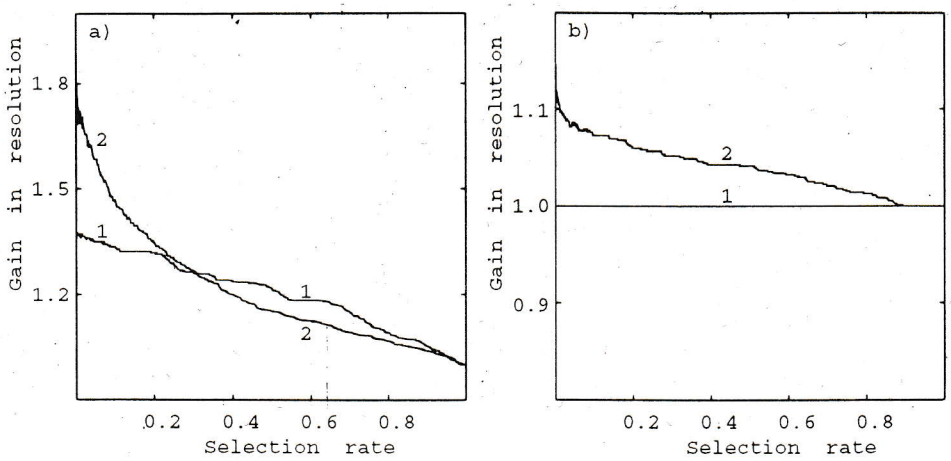


Figure 9: *Theoretical (1) and experimental (2) gain in the segments resolution as a function of the selection rate at $r_0$=3.12 cm (a) and $r_0$=11.6 cm (b).*

| $r_0$ | | $\tau = 100\%$ | $\tau = 10\%$ | $\tau = 3\%$ |
|---|---|---|---|---|
| 3.12 cm | Segmented aperture | 1.54 | 2.25 | 2.49 |
| | Full aperture | 1.31 | 1.53 | 1.66 |
| 11.6 cm | Segmented aperture | 1.22 | 1.30 | 1.33 |
| | Full aperture | 1.77 | 3.24 | 3.94 |

Table 2: *Gain in resolution for the segmentation system and the full pupil with image recentering at different selection rates $\tau$.*

tion are valid. The indicated acquisition procedure is applicable to fluxes as low as $\sim$ 2 photons per sub-aperture for autocorrelation functions, and $\sim$ 3 photons per sub-aperture for triple-correlation functions. This increases markedly the sensitivity of the technique.

As an example, in Fig.10 power spectra for the segmentation system and for the full aperture are shown with a flux equal to the total flux from individual segments. The squared spatial spectrum of centered non-selected images of $\gamma$ Vir from the results of the March observations are also given. Therein is also presented the signal/noise ratio for the corresponding power spectra and the relative errors of the squared spatial spectrum of the accumulated images. From the relationship presented it follows that the correlation signal acquisition for the segmentation system, compared to routine speckle interferometry, provides higher signal/noise ratio in comparison with ordinary acquisition, as well as higher signal/noise ratio near the atmospheric cut-off frequency. Besides, a higher signal/noise ratio of the segmentation system, both the ordinary and correlative acquisition, makes it possible to essentially increase the exposure time.

## 8. Conclusion

Thus, as a result of this investigation, it is practically shown that the angular resolution of the telescope can be significantly (up to 2 times) improved by using the pupil segmentation system even for the sites with moderate seeing conditions. The experiments were carried out to estimate a possibility of obtaining images with this system at the site of BTA telescope. Application of the pupil segmentation at BTA is problematic in the optical region (the optimum size of the segments is only 22 cm under 2″ seeing), but the method is very intresting in the infrared (at 2.2 $\mu$m the segment size is already 1.1 m).

The pupil segmentation in conjunction with the correlation techniques occupies an intermediate position between the ordinary image acquisition and interferometric imaging. On the one hand, it provides a higher spatial resolution in comparison with classical direct acquisition with the full aperture. Alternatively, the possibility of increasing the exposure time, decreasing equivalent focal length of the system and widening of the spectral range raise considerably sensitivity as against the interferometric techniques.

**Acknowledgements.** This work was partially supported by the grants No.1.4.1.3 and No.1.4.2.4 of the Russian Federation Programme "Astronomy".

## References

Balega Yu.Yu., Ryadchenko V.P., 1984, Pis'ma Astron. Zh., **10**, 229

Fried D.L., 1966, J. Opt. Soc. Am., **56**, 1380

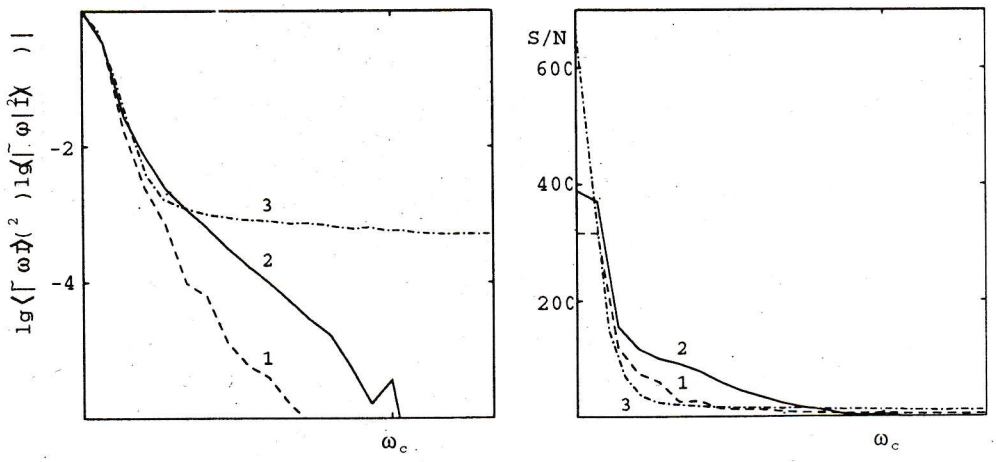


Figure 10: *The squared spatial spectrum of the averaged image (1), the power spectra for the segmentation system (2) and for the 1 m aperture (3) and their associated signal-to-noise ratios along the fringes of the spectrum of $\gamma$ Vir. The segment cut-off frequency $\omega_c$ is shown. No selection is applied.*

Fried D.L., 1978, J. Opt. Soc. Am., **68**, 1651
Hequet G., Coupinot G., 1985, J. Opt. (Paris), **16**, 21
Lelievre G., Nieto J.L., Salmon D., Llebaria A., Thouvenot E., Boulesteix J., Le Coarer E., Arnaud J., 1988, Astron. Astrophys., **200**, 301
Pluzhnik E.A., 1996, Astron. Zh., **73**, 146
Sebag J., Arnaud J., Lelievre G., Nieto J.L., Le Coarer E., 1990, J. Opt. Soc. Am. A, **7**, 1237
Tatarski V.I., 1967, Wave propagation in a turbulent medium, Moscow: Nauka, 548
Tokovinin A.A., 1988, Stellar interferometers, Moscow: Nauka, 160
Weigelt G., 1991, in: Wolf E. (ed.), Progress in Optics, **4**, 295